CALIFORNIA GEOLOGICAL SURVEY
FAULT EVALUATION REPORT FER-256

WEST NAPA FAULT
in the Napa and Cuttings Wharf 7.5-minute Quadrangles
Napa and Solano County, California

Ron Rubin
Engineering Geologist
January 11, 2018

INTRODUCTION

The August 24th, 2014 M_w 6.0 South Napa Earthquake (SNE) resulted in as much as 20 km of surface rupture on the West Napa Fault Zone (WNFZ) (Figure 1). Up to 50 cm of right-lateral displacement was observed on the principal rupture, with displacements of less than 10 cm on several parallel faults to the east, in a zone up to 2 km wide.

The WNFZ consists of a group of subparallel northwest-striking faults along the west margin of Napa Valley that accommodate a small portion of regional San Andreas Fault system dextral shear. Prior to the SNE, portions of the WNFZ had been evaluated for surface rupture potential in a Fault Evaluation Report (FER) by Bryant (1982), and portions of the fault in the American Canyon area were included in an Earthquake Fault Zone (EFZ) under the Alquist-Priolo Earthquake Fault Zoning Act (A-P Act).

Prior to the SNE, Bryant (1982) had mapped a significant portion of the fault that later ruptured as the principal trace of the SNE surface rupture; however, there was considerable uncertainty regarding both the activity of this principal fault trace, as well as the existence and activity of other faults within the WNFZ to the east. Consequently, mapped traces of the WNFZ in this area were not recommended for inclusion in an EFZ by Bryant (1982).

Combined with the pre-earthquake mapping of Bryant (1982), the 2014 SNE surface rupture provides an important calibration event by demonstrating how active traces of the WNFZ are geomorphically expressed. This informs a re-evaluation of the WNFZ for the faults that had not been previously included in an EFZ and either ruptured with minor displacements or did not rupture during the SNE.

The focus of WNFZ active fault mapping efforts (i.e., Wesling and Hanson, 2008; Bryant, 1982) and site specific subsurface investigations by numerous consultants and researchers (Clahan et al., 2011; Rubin et al., 2014) prior to the SNE, has been along faults on the west margin of the Napa Valley, termed here the West Napa Range-front Faults (WNRF). This zone generally follows the trend of the previously established EFZ in the Cuttings Wharf Quadrangle near the Napa County Airport. This FER addresses both the SNE ruptures, as well as the WNRF.

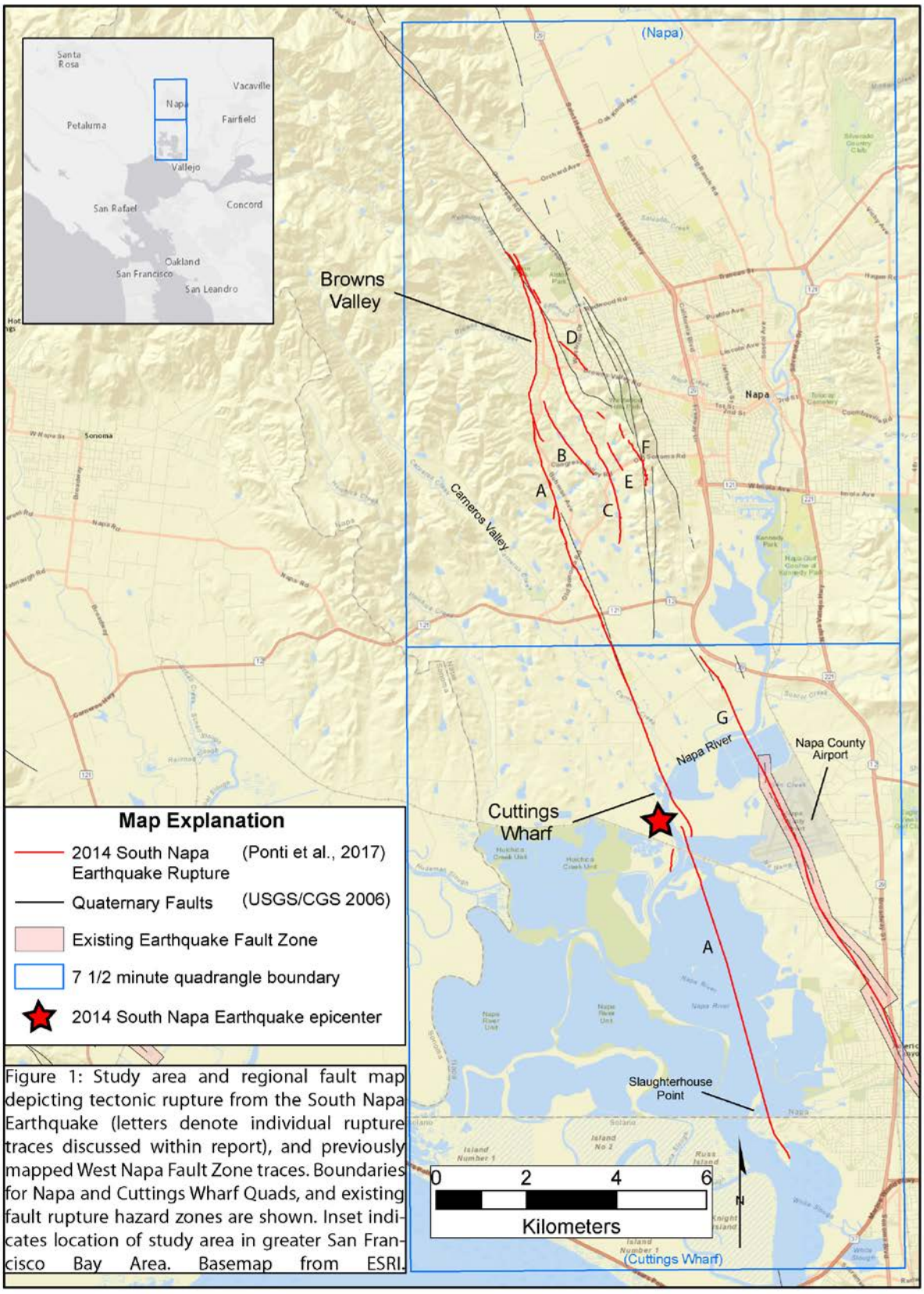

Figure 1: Study area and regional fault map depicting tectonic rupture from the South Napa Earthquake (letters denote individual rupture traces discussed within report), and previously mapped West Napa Fault Zone traces. Boundaries for Napa and Cuttings Wharf Quads, and existing fault rupture hazard zones are shown. Inset indicates location of study area in greater San Francisco Bay Area. Basemap from ESRI.

This evaluation employs new techniques and data sets that were not previously available, most notably lidar and synthetic aperture radar (SAR). These methods have greatly improved the ability to recognize active faults and detect surface deformation, even where no surface rupture or discontinuous surface ruptures are observed in the field. Post-SNE SAR data have enabled identification of previously unknown active faults, and have highlighted previously mapped faults that may be active. Additionally, this evaluation utilizes a more comprehensive compilation of geologic site investigations, aerial imagery, and original mapping.

This FER has two primary contributions: 1) Observations and new insights from the 2014 SNE surface rupture are combined with the other data for an improved understanding of the geomorphologic expression, location, and activity of the WNFZ; and 2) Recommendations that some faults along the previously un-zoned WNRF as well as all SNE rupture traces, be included in EFZ's.

For complete definitions of the criteria and specific language of the A-P Act and Policies of the State Mining and Geology Board (SMGB) related to the A-P Act, see Bryant and Hart (2007). Modification of the existing EFZ in the Cuttings Wharf Quadrangle near the Napa County Airport and to the south, will be addressed in a future separate FER.

SYNOPSIS OF THE 2014 SOUTH NAPA EARTHQUAKE RUPTURE

The M_w 6.0 South Napa Earthquake (SNE) occurred on the morning of August 24th, 2014 with the epicenter located near Cuttings Wharf at the mouth of the Napa River, approximately 2.5 km west of the Napa County Airport (Figure 1). The rupture occurred along seven individual traces, labelled A-G, spanning west to east, respectively, across a zone with a maximum width of approximately 2 km (Figure 1).

Trace A carries the majority of coseismic and all of the post-seismic slip from the SNE. Field evidence of surface rupture was documented north of the Napa River and continues northwest for about 12.5 km (Ponti et al., 2017). SAR imagery is used by Ponti et al. (2017) to extend the rupture mapping another 1 km northwest and 9 km southeast beyond the ends of rupture observed in the field. The maximum amount of measured coseismic net slip is 46 cm, which was observed approximately 9 km northwest of the epicenter along Trace A. Post-seismic slip occurred along Trace A south of Browns Valley, and after one year it nearly equaled the maximum coseismic slip (Lienkaemper et al., 2016).

Traces B – G (Figure 1) are subparallel to Trace A, and each have less measured displacement than Trace A. The maximum measured offset on Trace C is 7 cm and the maximum offset measured on other traces (B, D, E, F, G) did not exceed 6 cm. Post-seismic slip was not observed on Traces B – G.

The effects of the SNE rupture to cultural features are most apparent along Traces A, C, and D in the Browns Valley area, with widespread damage to streets, sidewalks, utilities, and residences (GEER, 2014; Hudnut et al., 2014). In general, measured displacements along Traces A and C in Browns Valley, range from 3 cm to 7 cm, with the maximum of 7 cm observed on Trace C. All of these rupture traces were mapped as through-going faults, although at a 1 m to 10 m scale,

gaps in the surface expression were observed. Several residential structures sustained extensive foundation damage from as little as 3 cm of measurable right-lateral rupture.

GEOMORPHIC EXPRESSION OF THE WEST NAPA FAULT ZONE

The occurrence of surface rupture along several faults that were not well-understood, or identified, prior to the SNE necessitates reconsidering the geomorphic expression of Holocene faulting in the Napa region. The WNFZ had previously been assessed with the expectation that Holocene faulting would be well-expressed with classic, through-going tectonic geomorphology such as right-lateral drainage offsets and scarps in Holocene deposits. This expectation may have been influenced by the lack of examples of moderate displacement surface ruptures, such as the SNE, on lower slip rate faults in the region. Therefore, comparing the geomorphic expression of faults that ruptured during the SNE with other mapped faults in the WNFZ, provides a valuable calibration for the geomorphic evidence of fault activity in the region.

Bryant (1982) dismissed some fault traces that ultimately ruptured in in the SNE based on their discontinuous and subdued geomorphic expression. However, evidence of pre-SNE, Holocene fault activity encountered in trenches along the rupture (e.g., Seitz et al., 2015; Dawson et al., 2016) are further examples of the limitations in characterizing the WNFZ with geomorphology alone. The current knowledge that these fault traces are Holocene active, with perhaps a weaker geomorphic expression than previously expected, also provides a basis for evaluating faults mapped by Wesling and Hanson (2008) along the western margin of Napa Valley.

Geomorphic expression of the WNFZ is evaluated in this FER by incorporating detailed air photo and lidar mapping, subsurface data, and extensive field checking. The results of lineament mapping are depicted on Plate 2 with numbered features corresponding to descriptions and evaluation comments in Table 1. Plate 2 incorporates lineament mapping both from this evaluation, as well as a subset of lineaments from Wesling and Hanson (2008). Features on Plate 2 mapped by Wesling and Hanson (2008) are generally limited to those which may be considered most likely to have a tectonic origin, such as through-going right-lateral offsets and scarps.

Details of the geomorphic mapping are addressed in the Evaluation and Discussion section below.

GEOLOGIC MAPPING OF THE WEST NAPA FAULT ZONE

The West Napa Fault Zone has been mapped extending from the Carquinez Strait to near St. Helena. Figure 1 locates the study area and depicts faults compiled into the Quaternary Fault and Fold Database by the United States Geological Survey and California Geological Survey (USGS/CGS, 2006), as well as the SNE rupture, and the existing EFZ.

The WNFZ is a right-lateral strike-slip fault, which is consistent with its strike being sub-parallel to the San Andreas fault system. Regionally, movement on the WNFZ has juxtaposed Cretaceous and Tertiary sedimentary rocks on the west with Tertiary Sonoma Volcanics on the east (Wagner and Gutierrez, 2016). Local exceptions to this relationship exist where traces of the fault are mapped entirely within Sonoma Volcanics or alluvium, or at the contact between bedrock and

alluvium. Brossy et al. (2010) and Catchings et al. (2016) suggest transfer of right-lateral slip northwestward from the Calaveras Fault to the West Napa Fault via the Contra Costa Shear Zone in the northern East Bay Hills.

Previous fault mapping efforts (Plate 1) within the Napa region have focused primarily along the western margin of Napa Valley (i.e., WNRF), and further west in the bedrock uplands and intermediate valleys between Napa Valley and Carneros Valley (Figure 1). Published mapping of the fault has been presented at various scales of 1:24,000 or smaller, and is generally based on regional observations. While some of this mapping focused on identifying active and potentially active faults (e.g., Helley and Herd, 1977; Pampeyan, 1979), other geologic maps (e.g., Fox et al., 1973; Wagner and Bortugno, 1982; Clahan et al., 2004; Graymer et al., 2007) focused on establishing the regional geologic framework with no implied inference of seismogenic capability. Portions of the earlier mapping are compiled within the Quaternary Fault and Fold Database (USGS/CGS, 2017).

The mapping of Bryant (1982) and Wesling and Hanson (2008), focus on recognizing recent tectonic features, at larger scales than previous work. Wagner and Gutierrez (2016) compiles much of the previous fault mapping, and incorporates an early version of the SNE rupture mapping provided in Hudnut et al. (2014), which has subsequently been superseded by Ponti et al. (2017).

PREVIOUS ASSESSMENTS OF FAULT ACTIVITY

Several prior reports (e.g., Fox et al., 1973; Helley and Herd, 1977; Pampeyan, 1979; Wesling and Hanson, 2008; and Clahan et al., 2011) concluded Holocene faulting was evident along portions of the range front of western Napa Valley, primarily based on a prominent scarp in eastern Alston Park and a shallow cross-fault stream exposure interpreted to expose evidence of multiple Holocene-age faulting events (e.g., Clahan et al., 2011; discussed further in later sections of this report, and in Table 2). Slip rate estimates on the WNF are poorly constrained, with estimates ranging from ≤1 to 4 mm/yr based largely on general geomorphology as well as models based on regional geodesy (e.g., Field et al., 2013).

A fault evaluation by Bryant (1982) addresses previously mapped fault traces of Fox et al. (1973), Helley and Herd (1977), and Herd (as depicted in Bryant, 1982). That evaluation utilized aerial imagery, field reconnaissance, and available fault investigation reports. Bryant (1982) noted a lack of displacement of young alluvial fans; lack of systematically deflected drainages; degraded/eroded scarp at Alston Park; and inconclusive evidence for Holocene faulting in several consulting trenches across mapped faults/geomorphic features. Based on these observations, Bryant concluded that the mapped faults were not considered sufficiently active or well-defined, and no EFZ was designated.

Wesling and Hanson (2008) mapped a system of active faults based on the geomorphic expression of features along the WNRF, and through the hills to the west (Plate 2, Table 1). This work is based primarily on aerial imagery and limited field reconnaissance. Wesling and Hanson (2008) map several geomorphic lineaments such as scarps and deflected drainages, and concluded these are fault-related. Holocene ages of faulting are interpreted and assigned to many of the mapped lineaments.

COINCIDENCE OF SOUTH NAPA EARTHQUAKE RUPTURE WITH PREVIOUS MAPPING

The 2014 South Napa Earthquake ruptures occurred in areas with several previously mapped bedrock faults (Plate 1) and poorly expressed geomorphic features (Plate 2), which were not well-understood prior to the earthquake. Trace A is located up to 3 km west of the WNRF and most of the previously mapped active faults, although it is roughly coincident with previous mapping of geologic faults, north of South Avenue. Traces C and F are coincident with previously-mapped faults for short distances, while Traces B, D, and E were unmapped prior to the SNE (Plate 1). Trace G is the only SNE rupture trace to clearly correspond with a previously recognized Holocene-active fault. Bryant (1982) included Trace G within an EFZ (Figure 1, and Plate 1) based on relatively clear geomorphic expression and available subsurface data in the area of the Napa County Airport and to the south.

Bryant (1982) had mapped approximately 4 km of Trace A consisting of two separate sections, including the portion with the highest coseismic slip in the SNE, based on geomorphic expression. Despite noting features such as sharp tonal lineaments, linear drainages, saddles, and two right-laterally deflected drainages, Bryant concluded that the relatively subdued geomorphic expression cast doubt on the origin and recency of the features and thus did not recommend those faults for inclusion in EFZ's. This may be due, in part, to the lack of subsurface data at the time and an apparent bias towards analogous examples of active fault geomorphology from higher slip rate faults that typically exhibit systematically deflected drainages and sharp scarps in young materials.

The occurrence of the SNE rupture, along with recent subsurface data demonstrate the fault does in fact meet A-P Act criteria of "sufficiently active" and, with the hindsight of experience and a recalibrated understanding of active fault geomorphology, the criteria of "well-defined".

USE OF SAR IMAGERY

Synthetic aperture radar (SAR) can provide strong evidence for both location and activity of faults by measuring ground surface changes on the order of centimeters (cm), when data from repeated surveys are differenced. This method is uniquely suited to assessing tectonic ground deformation because it collects images on a regional scale, and often at temporal intervals that allow the differentiation of coseismic and post-seismic deformation. SAR data collected with a space-borne method, are commonly referred to as InSAR (Interferometric Synthetic Aperture Radar). A variation of SAR that uses airborne methods is known as UAVSAR (Unoccupied Aerial Vehicle Synthetic Aperture Radar). For background on SAR concepts see Jones (2015).

The National Aeronautics and Space Administration's (NASA) Jet Propulsion Laboratory (JPL) has an on-going UAVSAR mission over northern California as part of an experiment to record movement along major elements of the San Andreas fault system. In the days after the SNE, JPL was able to deploy their UAVSAR system and collect post-earthquake data that provided insights into both the spatial and temporal distribution of coseismic and post-seismic movement along the WNFZ. Within a week of the SNE, SAR imagery became available and clearly imaged the SNE rupture and confirmed its distributed nature along multiple subparallel faults. An example

of the utility of SAR data was the recognition of through-going deformation along Traces B, D, and G, which had not been clear during initial field mapping.

As a complementary tool to field mapping, Ponti et al. (2017) extensively utilized JPL's UAVSAR data to map the SNE rupture. They classify SAR lineaments into two categories of origin: "tectonic" and "uncertain" (Plate 4). According to Ponti et al. (2017), the criteria for a tectonic origin is coincidence with, or connection between points of field-confirmed tectonic rupture, as well as projections on-trend beyond the end of field-confirmed tectonic rupture. The uncertain category consists of SAR lineaments that cannot be clearly associated with tectonic surface ruptures due to a lack of evidence of rupture observed in the field, the lineament being isolated spatially, inconclusive results in analysis of line-of-sight displacements (e.g., Donnellan et al., 2015; DeLong et al., 2016), or other limitations.

The lack of observed rupture in the field (Ponti et al., 2017) along several interpreted SAR lineaments in Napa is apparently in contrast to experiences following the 2010 El Mayor-Cucapah Earthquake in the Yuha Desert (e.g., Treiman, 2012). Treiman (2012) reports the SAR imagery reliably captured minor amounts of visible surficial deformation; however, only a limited number of SAR lineaments in the Yuha Desert were field-checked whereas in Napa, the vast majority were field-checked by multiple observers.

Possible explanations for the differences between the outcomes of SAR-based mapping of the El Mayor-Cucapah Earthquake and SNE include environmental characteristics such as a lack of vegetation and ideal surface conditions amenable to recording minor displacements in the arid region of the El Mayor-Cucapah rupture. Those ruptures had cm-scale displacements and were observable both on the UAVSAR as well as in the field. However, they are likely below the threshold of what can be reliably be observed in northern California, where vegetation and soil properties may inhibit the expression of fault ruptures with small displacements.

In this FER, lineaments mapped by Ponti et al. (2017) using SAR are evaluated such that the lineaments are accepted as active faults when they meet any of the following criteria:

- Lineament is coincident with fault rupture observed in field.
- Lineament extends from, or is on trend with observed fault rupture.
- Lineament exhibits post-seismic slip as observed on post-earthquake pairs of imagery.
- Lineament is coincident with a previously mapped active fault.
- Lineament is coincident with pre-existing geomorphic features that may be indicative of faulting.
- Lineament is coincident with subsurface trench data.
- Lineament is consistent with plausible structural relationships to known active faults.

A possible limitation with the use of SAR imagery is that some lineaments with non-tectonic origins may be expressed as linear features, which could be mistaken for faulting. Such features have

been ascribed to known phenomena that affect SAR data such as: atmospheric distortion, groundwater fluctuations, vegetation changes, differential subsidence of variable subsurface materials along discontinuities or strength contrasts, incoherence/decorrelation of SAR data, effects of soil moisture, or others (e.g., Rosen et al., 2006; Zwieback et al., 2015; DeLong et al., 2016). Another possible origin of "uncertain" SAR features described in Ponti et al. (2017) could include tectonic movement on blind structures (DeLong et al., 2016). All of these various sources of SAR signals could indicate a cm-scale range movement (Rosen et al., 2006), and may account for the uncertain origin of some of the SAR lineaments mapped by Ponti et al. (2017).

With awareness of uncertainties in SAR data, the criteria for activity listed above are intended to specifically identify SAR lineaments plausibly related to surface or near-surface faulting. SAR features related to other non-tectonic origins are unlikely to be coincident with lineaments mapped using these criteria. Furthermore, the experience following the SNE, where mapped SAR lineaments were later field checked and cm-scale displacements were found across fragile cultural features, gives additional confidence that the SAR lineaments mapped using these criteria are fault related. As with the El Mayor-Cucapah Earthquake UAVSAR-based mapping of Treiman (2012), the SNE example shows that UAVSAR can reliably identify faults with minor displacements that may only be detectable on the ground in ideal conditions.

EVALUATION AND DISCUSSION

In the sections below, evaluation of SNE rupture mapping is presented first, followed by evaluation of WNRF's mapped prior to the SNE.

Evaluation of SNE Rupture Mapping

This section evaluates the mapping of SNE rupture Traces A-G by Ponti et al. (2017), which presents the results of field mapping from many contributors, and interpolates connections between field observation points, as well as interpretations of SAR lineaments, lidar and imagery. It is the most comprehensive record of surface rupture observations associated with the SNE. In the evaluation below, discussion of imagery, previous mapping, and site investigations are incorporated where instructive.

Based on the overall consistency of field evidence indicating through-going, right-lateral surface displacement along km-scale sections of the ruptures, faults mapped by Ponti et al. (2017) (e.g., Plates 1-4) are considered active. Where Ponti et al. (2017) designates an inferred origin, that convention is generally maintained in this evaluation. In this section, descriptions of SNE mapping, offset measurements, and UAVSAR interpretations related to the SNE rupture are from Ponti et al. (2017) unless otherwise noted.

For ease of discussion, the following discussion is arranged in sections from south to north relative to features labelled on Plates 1 through 5. The results of the fault evaluation are depicted on Plate 5.

Slaughterhouse Point to Highway 12

This area includes Traces A, C, and G, west to east, respectively. Trace A south of the Napa River is characterized by a clear expression in both coseismic and post-seismic SAR imagery. The SAR lineament is aligned on-trend with Trace A north of Napa River (Plate 4; Ponti et al., 2017). Some field observations south of the Napa River further support rupture during the SNE. The post-seismic SAR imagery is significant because it records continued fault movement along the same alignment as the co-seismic imagery.

Further supporting evidence for activity on the southern-most section of Trace A includes studies of the SNE's seismicity and subsequent geodetic modeling (e.g., Dreger et al., 2015; Melgar et al., 2015), which suggests shallow slip extends south of the SNE epicenter to an extent approximately similar to the rupture mapping of Ponti et al. (2017). The majority of this section of Trace A is submerged, or within inaccessible wetlands, and therefore lacks the density of field observations similar to the sections of Trace A north of the Napa River. Based on its strong expression on both co-seismic and post-seismic SAR imagery, and its orientation on-trend with Trace A north of the Napa River, this portion of the fault is considered active (Plate 5).

North of Napa River, the rupture along Trace A is characterized by right-lateral offsets on pavement, offset vineyard rows, as well as en echelon cracks in soil. Displacements measured in the field range up approximately 20 cm or more, with a local vertical component. Total slip, including post-seismic slip in this area reaches a maximum of 49 cm (Lienkaemper et al., 2016). Pre-existing geomorphology consists of an east-facing, approximately 7-m-high scarp (Features 1 and 4; Plate 2 and Table 1) previously recognized by Bryant (1982) and Wesling and Hanson (2008). Bryant (1982) notes cultural modification may have artificially enhanced the sharpness of the scarp, and did not consider the scarp to be conclusive evidence of Holocene faulting. A trench across the rupture at Site 2 (Plate 3 and Table 2) exposes a pre-SNE deformation zone with stratigraphic juxtaposition of alluvial deposits across it. This provides clear evidence of a through-going fault zone with a prior history of displacement along this section of the fault, which includes the scarp previously noted at Features 1 and 4 (Plate 2).

Approximately 2.1 km south of Highway 12, Ponti et al. (2017) characterize Trace C with an alignment of several SAR lineaments (Plate 4). This section of Trace C is on-trend with observed rupture to the north, and could represent a structure that transfers slip from Trace C to Trace G. Elevated topography between these traces is consistent with a restraining step across these faults. Ponti et al. (2017) interpret an uncertain origin for this section of the fault, which is consistent with a lack of observed SNE rupture in the field and a lack of clear tectonic geomorphic features. However, based on the relatively clear alignment with the rupture to the north, it appears these lineaments represent the southern continuation of Trace C and are considered active.

Trace G, the eastern-most rupture along the SNE rupture provides insights into the location and possible continuity of the rupture with previously mapped faults. This portion of the rupture lies in proximity to the fault mapped by Bryant (1982), and extends that fault over 2.5 km northwest from the existing EFZ (Plate 5). The northwest extension of the fault is mapped on-trend from the documented rupture at the Napa Airport, based primarily on UAVSAR (Plate 4; Ponti et al., 2017). The location and general trend of Trace G could also be consistent with a right-stepping

relationship to the WNRF. Based on the expression in SAR imagery and field observations of faulting at the Napa Airport, the northwestern extent of Trace G is considered active (Plate 5).

Highway 12 to Browns Valley Road

Traces A, B, C, E, and F are mapped in this area, west to east, respectively. The rupture along Trace A in this area is continuous with the section to south, and is characterized by right-lateral offsets to pavement, curbs, and vineyard rows, as well as expressed as fissures, en echelon cracks and mole tracks. Locally, displacement is accommodated over a width of up to 14 m. The maximum right-lateral displacement of 44 cm is measured at a point approximately 4 km north of Highway 12. Pre-existing geomorphology consists of an east-facing scarp, linear front, and linear valley, saddles, as well as two right-lateral drainage offsets (2.4 and 3.7 km north of Highway 12) which were noted by Bryant (1982), who mapped approximately half of this reach of Trace A.

Bryant (1982) did not conclude that the geomorphic features mapped along what is currently recognized as Trace A were the result of active faulting, instead reasoning they were more likely the result of differential erosion. Bryant also noted the lack of geomorphic features south of Henry Road, which, if present, would have provided a connection with the scarp south of Highway 12. With perspective from the SNE rupture and paleoseismic evidence from post-SNE trenching studies along Trace A (e.g., Sites 2 and 4; Plate 3), it is reasonable to conclude that the previous fault evaluations such as Bryant (1982) may have been biased by an expectation of well-developed tectonic geomorphology, as well as a lack of available subsurface data with constraints on the timing of past faulting.

Trace B is approximately 2 km long, and the rupture is expressed as the deformation and cracking of pavement and sidewalks/curbs (Plate 1). Offsets are less than 1 cm, and include right-lateral, left-lateral, and vertical offsets. Geomorphic evidence of Trace B was not recognized in Bryant (1982), nor is it observed in this evaluation using aerial and lidar imagery.

Trace C is the second longest rupture trace for a total length of about 7 km. From its northward continuation starting at Highway 12, it is mapped for approximately 1 km based on discontinuous SAR lineaments (Ponti et al., 2017; also see Plate 4). Mapping for this FER infers a connection between the SAR lineaments to the portion of Trace C with field observations of SNE surface rupture (Plate 5). Rupture observations along Trace C include right-lateral offsets, en echelon cracks, and fractures across cultural features and in soil. The width of deformation was observed to be up to 20 m, with a maximum right-lateral displacement of approximately 5 cm. Trace C roughly follows fault-parallel north-northwest trending valleys. Geomorphic features clearly related to active faulting are not observed using lidar or pre-development aerial photographs in this evaluation. A trench exposure across the rupture at Site 5 (Plate 3 and Table 2) depicts a flower structure approximately 2 m wide (RGH Consultants, 2015b). This deformation suggests a longer history of fault activity and possibly greater displacement than what is documented from the SNE; although that topic is not specifically addressed in the report by RGH Consultants (2015b).

Trace E is mapped by Ponti et al. (2017) as three separated sections. The southern-most section is expressed as en echelon cracks, with right- and left- lateral offsets and a maximum measured

offset of 5 cm. Pre-SNE geomorphology consists of a saddle (Feature 37; Plate 2 and Table 1) along the southern section. The northern two sections are characterized by discontinuous cracks, some with extensional measurements.

Surface rupture on Trace F is expressed by cracks with right-lateral and up-on-the-west vertical components, over a distance of approximately 1.5 km (Ponti et al., 2017). Maximum right-lateral displacements are 5 cm with lesser vertical. Pre-SNE geomorphology includes an alignment of saddles, linear valleys, and side hill benches west of the ridgeline (Plate 2 and Table 1).

Trace F as-mapped by Ponti et al. (2017) was not recognized prior to the SNE; however, other faults had been mapped nearby (Plate 2). Trenches at Site 7 (Plate 3 and Table 2) have clarified the presence or absence of those previously mapped faults, and the timing of activity. A previously mapped fault along the western portion of the site was encountered within several trenches, and determined by a consultant to have pre-Holocene movement based on the age of faulted deposits in the lower portion of Trench 6 (Berlogar Stevens and Associates, 2014). However, deformation extends upwards to within approximately 2 feet of the ground surface in undated deposits. Due to the faults' proximity to within in a few meters of the SNE rupture along the north end of Site 7, the consultant recommended a fault set back from this fault. Trenches across other previously-mapped faults and geomorphic features at Site 7 encountered no evidence of faulting (e.g., Phoenix Geotechnical, 1994; 1998).

Trench investigations across Trace F at Site 7 (Plate 3 and Table 2) following the SNE provide evidence for two to three prior Holocene ruptures (Seitz et al., 2015; and Seitz pers. comm. 2017). The earlier ruptures have apparent vertical displacements significantly larger than in the SNE (Seitz et al., 2015), suggesting Trace F may have a greater spatial extent than exhibited by the relatively short length of its SNE rupture. Consequently, geomorphic features such as a saddle and linear valleys (Features 14, 18, 19, and 22; Plate 2) and a UAVSAR lineament recognized in this evaluation to the southeast along the trend of Trace F, are used to map Trace F approximately 1 km farther southeast than Ponti et al. (2017) indicate (Plate 5).

Post-SNE observations at the north end of Trace F indicate the rupture could not be mapped beyond the northernmost field checked observation (Plate 4). Observations northeast of that location include E- NE-trending ground cracks, and a SAR lineament is coincident with some of these field observations (Ponti et al., 2017). This area is located within a mapped landslide (Wagner and Gutierrez, 2016). The inconsistent trend of the cracks with the rest of the rupture, and their location within a mapped landslide suggests that these features may be related to gravity-driven processes of the landslide. However, a tectonic origin cannot be ruled out, and is equally plausible given these features are seen both in the field and in SAR imagery, and could represent an extension of Trace F (Plate 5).

<u>Browns Valley, between Browns Valley Road and Redwood Road</u>

SNE ruptures along Trace A, C, and D in Browns Valley resulted in the highest concentration of damage as a direct result of surface rupture. Several residential structures sustained extensive damage despite the maximum displacements being relatively small, on the order of <10 cm. Traces A and C ruptures are expressed as en echelon cracks in pavement, offset curbs, distress

to foundations and walls of structures, and broken underground utilities. Measured displacements range up to approximately to 7 cm on both Traces A and C, and generally decrease northward to 3 cm. Geomorphic features along the rupture are not observed in pre-development aerial photographs and lidar imagery along Trace A.

Trace D is approximately 1-km-long and mapped by Ponti et al. (2017) across the central area of Browns Valley based on field observations coincident with a SAR lineament (Plate 4). Deformation is expressed as an alignment of deformed cultural features including en echelon cracks in pavement, right-lateral offset curbs, and broken sidewalk panels. Measured right-lateral displacements of 1 to 2 cm are reported in Ponti et al. (2017). An isolated hill within the valley floor, which is bounded by Trace C on the west, has a steep eastern face that is on trend with Trace D, and may represent a pre-existing localized uplift between Traces C and D. Based on the reported field observations and possible geomorphic expression, Trace D is inferred to extend beyond the mapping of Ponti et al. (2017) approximately 200 m to the northwest in this evaluation (Plate 5).

Redwood Road to north end of rupture

This area includes Traces A and C. Both traces are recognized as continuous features; although, Trace C is more clearly mappable as a through-going feature for a greater overall length, with larger displacements relative to Trace A. The rupture is expressed as fissures and en echelon cracks in soil and pavement. Measured displacements are 3 cm at Redwood Road and decrease toward the north end of the rupture, although a displacement of 6 cm is measured on Trace C approximately 1 km north of Redwood Road. A horse corral fence and a house at the Hendry winery exhibit displacements on the order of centimeters. Pre-existing geomorphology generally consists of scarps in an elevated, likely Pleistocene or older terrace surface (Features 67 and 68; Plate 2). Trenches across the ruptures on this elevated surface expose evidence of prior displacements (Site 24; Plate 3 and Table 2). The minimum age of these displacements are only constrained by trenches across the ruptures on lower surfaces, which expose no evidence of prior displacements within approximately 6,000-year-old deposits (Prentice et al., 2015).

Approximately 1 and 1.3 km north of Redwood Road (for Traces A and C, respectively) to the northern termination of the rupture as mapped by Ponti et al. (2017), the rupture is weakly expressed, and Ponti et al. (2017) rely on SAR to extend the mapping (Plate 4). Ponti et al. (2017) also map a complex zone of ridgetop fissures at the north end of Trace C; however, they conclude the fissures showed no evidence of right-lateral movement and indicate the SAR lineaments have an uncertain origin. Several trenches were opened across a SAR lineament and fissures following the SNE at Site 28 (Plate 3), and evidence of previous deformation was not encountered (Table 2). However, the on-trend continuity of the SAR lineaments (as mapped by Ponti et al., 2017) and the observations of rupture to the south, as well as the concentrated fissuring in this area, suggest the possibility that portions of these features could be fault-related. Therefore, this portion of the rupture is considered active (Plate 5).

Evaluation of Pre-2014 Fault Mapping and Site Investigations

This section evaluates fault mapping and subsurface site investigations completed prior to the SNE. Geomorphic mapping conducted as part of this evaluation, as well as post-SNE SAR-based mapping and subsurface investigations are also discussed where they inform conclusions in this evaluation. This section focuses on the boundary between the valley floor of Napa Valley and bedrock uplands to the west, where much of the pre-SNE WNRF mapping and site investigations were focused.

The discussion is arranged in sections from south to north relative to roads labelled on Plates 1-5. A summary of subsurface investigations is provided in Table 2. Locations of site investigations are shown on Plate 3.

Highway 12 to Browns Valley Road

The western margin of Napa Valley consists of a linear, east-facing range front extending northwest from near the intersection of Highways 12 and 29, valley floor topography in western Napa Valley meets bedrock uplands on the west (Plate 1). Wagner and Gutierrez (2016) depict a number of faults along this boundary, and Wesling and Hanson (2008) map a series of discontinuous, Holocene or probable Holocene faults along the base of the east-facing bedrock hills (Plate 1). These faults are considered part of the WNRF. Evaluation of faults in this area is based on geomorphology and subsurface data, as well as SAR lineaments.

Geomorphology in this area consists primarily of east-facing scarps and linear fronts (Plate 2 and Table 1). Mapping for this FER finds similar features to those mapped by Wesling and Hanson (2008), although the locations are considered more accurate because of the use of high resolution lidar imagery, which was not available previously. The differences in interpretation are generally related to the location and extent of some features.

The strongest geomorphic features are expressed at the southeast and northwest ends of this area. At the southeast end, an approximately 1 km long scarp is mapped beginning southeast of Highway 29 (Features 5 and 7; Plate 2 and Table 1). A SAR lineament mapped by Ponti et al. (2017) (Plate 4) is coincident with Feature 7 (Plate 2 and Table 1), and extends northwest approximately 0.6 km. Post-SNE field observations along the SAR lineament and scarp did not identify evidence of rupture, and Ponti et al. (2017) indicate the lineament has an uncertain origin. Nevertheless, the coincidence of the SAR lineament with the geomorphic scarp is considered evidence of activity.

Between approximately 2 and 3 km north of Highway 12 the fault is inferred along the bedrock slopes based on a continuous linear scarp visible in lidar hillshade and slopeshade imagery (Feature 23; Plate 2 and Table 1). Though it is difficult to distinguish active fault scarps from scarps formed by differential erosion along this section (as well as in other areas discussed below), supporting evidence of activity exists on adjacent sections of the fault. At the northeast end of this area, a series of linear fronts and scarps (Features 46, 49, and 50; Plate 2 and Table 1) characterize a 1 km-long section terminating at Browns Valley Road.

Several site investigations have excavated trenches across previously mapped and suspected active faults in the area. Sites 6, 10 and 12 (Plate 3 and Table 2) encountered faults, with Site 12 exposing a fault breaking the bedrock/soil interface. Feature 49 (Plate 2) is mapped coincident with the fault at Site 12. Mapped faults were not encountered at Sites 7, 8, 9, and 11 (Plate 3 and Table 2).

Based on the trench at Site 12 exposing faulted soil, strong geomorphic expression at the ends, coincident SAR lineaments, continuity with the section to the northwest, and plausible continuity from the south across a stepover from Trace G, faults shown on Plate 5 in this area are considered active.

Browns Valley Road to Redwood Road

An elongate set of northwest- southeast-trending, fault-bounded hills (e.g., Wagner and Gutierrez, 2016; Wesling and Hanson, 2008) (Plates 1 and 2) separates Browns Valley and Napa Valley. Evaluation of faults along the west-facing slopes is based on geomorphology and subsurface data, whereas faults along the east-facing slopes are based on geomorphology with a SAR lineament.

Geomorphic features in this area consist primarily of linear fronts and saddles (Plate 2 and Table 1), similar to features in Wesling and Hanson (2008); although, a right deflected drainage (Feature 54; Plate 2 and Table 1) mapped by Wesling and Hanson (2008), could not be identified in pre-development aerial photographs. A SAR lineament mapped by Ponti et al. (2017) is largely coincident with a linear front and linear drainage (an example is Feature 53; Plate 2 and Table 1) along a portion of the eastern hill front (Plate 4). Ponti et al. (2017) indicate the lineament has an uncertain origin, but it may be consistent with a small amount of tectonic or triggered movement.

Several previously mapped faults in the area have been investigated with trenches, and evidence of faulting was interpreted by consultants in trenches at Sites 16, 18, and 19 (Plate 3 and Table 2). Sites 18 and 19 expose faults within bedrock that break the bedrock/soil interface, which is considered strong evidence of activity. Faults were not recognized by the consultants at Sites 13, 17, 19, 21 and 22 (Plate 3 and Table 2). However, the log from Trench 4 at Site 17 (Plate 3 and Table 2), depicts shears in a location that is generally on trend with a fault found at Site 16, and thus are permissive of faulting. Site 14 (Plate 3 and Table 2) represents a natural creek exposure where Wesling and Hanson (2008) logged and dated a fault as extending upward into young alluvium; however, critical relations on the log could not be reproduced in visits to the site as part of this evaluation.

Based on trench exposures of faulted soils, and the continuity of geomorphic expression with adjacent areas, uplifted topography, and a coincident SAR lineament, faults shown on Plate 5 in this area are considered active.

Redwood Road to Linda Vista Ave

Napa Valley and bedrock uplands to the west are separated by low hills through which faults have been mapped, north of Redwood Road (e.g., Wagner and Gutierrez, 2016; Wesling and Hanson,

2008). Evaluation of faults in this area is based on geomorphology, subsurface data, and a SAR lineament.

Geomorphic features in this area include scarps and a right-lateral drainage offset. The most prominent feature is a scarp just north of Redwood Road (Feature 66; Plate 2 and Table 1) in eastern Alston Park. The scarp is considered evidence of recent fault activity on several maps (e.g., Fox et al., 1973; Helley and Herd, 1977; Wesling and Hanson, 2008; Clahan et al., 2011). Mapping the location of this section of the fault is informed by trenches (Sites 25 and 26; Plate 3 and Table 2) across Features 66 and 73 (Plate 2 and Table 1) that did not expose faults. Subsurface data are not available for other geomorphic features in the area. However, SAR lineaments (Figure 4) and post-SNE observations (Ponti et al., 2017) along portions of the scarp suggest an unknown amount and direction of movement related to the SNE. Plate 5 depicts a fault in this area that reflects

A second scarp (Feature 72; Plate 2) in the area extends from 1.8 km to 2.2 km northwest of Redwood Road, along Dry Creek Road, and lidar profiles reveal it separates higher and lower surfaces in the approximate location of the road. A right-lateral drainage offset along Feature 72 0.2 km southeast of Linda Vista Avenue can be seen in lidar and early aerial photographs where the drainage crosses Dry Creek Road. Feature 72 represents the approximate northern limit of well-defined geomorphic features. Additional evidence of active faults beyond this point may be obscured by more youthful alluvial features. Regional geologic mapping depicts concealed and inferred faults (Plate 1; Wagner and Gutierrez, 2016) further northwest along Dry Creek Road. In the northwest corner of the Napa Quadrangle the fault is shown to separate bedrock formations; however, tectonic geomorphic features are not observed in this area.

Within the valley floor, several previously mapped geomorphic features northeast of Dry Creek Road (Wesling and Hanson, 2008) were either not observed or not interpreted as likely of tectonic origin in this evaluation (i.e., they could not be validated). See Plate 2 and Table 1 for details of these features.

Based on the strong expression of scarps and a right-lateral offset along Dry Creek Road, the continuity of geomorphic expression on trend from south of Redwood Road, uplifted topography, and a coincident SAR lineament, faults on Plate 5 in this area are considered active.

RECOMMENDATIONS

Recommendations for including faults within EFZ's are based on the criteria of "sufficiently active" and "well-defined" (Bryant and Hart, 2007). The principal traces of the West Napa Fault Zone evaluated in this report are shown on Plate 5, and are recommended for inclusion within EFZ's as they are considered to be sufficiently active and well-defined.

Ron S. Rubin P.G. 7730, C.E.G. 2488

Engineering Geologist

Reviewed and approved:

Timothy E. Dawson P.G. 8502, C.E.G. 2618

Senior Engineering Geologist

January 11, 2018

REFERENCES CITED

Berlogar Stevens Associates, 2014, Fault Investigation Report, Napa Oaks, Old Sonoma Road, Napa, California, Job Number: 3280.002, dated December, 9 2014.

Bray, J., Cohen-Waeber, J., Dawson, T., Kishida T., and Sitar, N. (Editors), 2014, Geotechnical Engineering Reconnaissance of the August 24, 2014 M 6 South Napa earthquake, Geotechnical Extreme Events Reconnaissance Association Report GEER-037, 415 pp.

Brocher, T., Baltay, A., Hardebeck, J., Pollitz, F., Murray, J., Llenos, A., Schwartz, D., Blair, J., Ponti, D., Lienkaemper, J., Langenheim, V., Dawson, T., Knudsen, K., Shelly, D., Dreger, D., Boatwright, J., Aagaard, B., Wald, D., Allen, R., Barnhart, W., Brooks, B., and Scharer, K., 2015, The M-W 6.0 24 August 2014 South Napa Earthquake: Seismological Research Letters, v. 86, no. 2, p. 309-326.

Brossy, C., K. Kelson, and M. Ticci (2010), Digital Compilation of Data for the Contra Costa 470 Shear Zone for the Northern California Quaternary Fault Map Database: Collaborative Research with William Lettis & Associates, Inc. and the U.S. Geological Survey: Final Technical Report submitted to the U.S. Geological Survey NEHRP, Award no.07HQGR0063.

Bryant, W.A., 1982, West Napa fault zone and Soda Creek (east Napa) fault, Napa County: California Division of Mines and Geology Fault Evaluation Report FER-129, 9 p. *in* Fault Evaluation Reports Prepared Under the Alquist-Priolo Earthquake Fault Zoning Act, Region 1 – Central California: California Geological Survey CGS CD 2002-01 (2002).

Bryant, W.A., and Hart, E.W., 2007, Fault-rupture hazard zones in California: California Geological Survey Special Publication 42 (Interim Revision 2007), 42 p. (digital version only, electronic document, available at ftp://ftp.consrv.ca.gov/pub/dmg/pubs/sp/Sp42.pdf).

Catchings, R. D., Goldman, M. R., Li, Y. G., and Chan, J. H., 2016, Continuity of the West Napa-Franklin fault zone inferred from guided waves generated by earthquakes following the 24 August 2014 M_W 6.0 South Napa Earthquake: Bulletin of the Seismological Society of America, v. 106, no. 6, p. 2721–2746.

Clahan, K.B., Wagner, D.L., Saucedo, G.J., Randolph-Loar, C.E., and Sowers, J.M., 2004, Geologic map of the Napa 7.5′ Quadrangle, Napa County, California: A digital database: California Geological Survey, scale 1:24,000.

Clahan, K.B., Wesling, J.R., and Brossy, C., 2011, Paleoearthquake Chronology along the Northern West Napa Fault Zone, Napa County, California: Final Technical Report submitted to the U.S. Geological Survey NEHRP, Award no. 07HQGR0081.

Dawson, T.E., Rubin., R.S., and Mareschal, M., 2016, Paleoseismic Results from Two Sites on the Principal Strand of the August 24, 2014 South Napa Earthquake Rupture: Seismological Research Letters, v. 87, n. 2B, p. 536.

DeLong, S., J. Lienkaemper, A. Pickering, and N. Avdievitch, 2015, Rates and patterns of surface deformation from laser scanning following the South Napa earthquake, California: Geosphere, v. 11, n. 6, p. 2015–2030.

DeLong, S.B., Donnellan, A., Ponti, D.J., Rubin, R.S., Lienkaemper, J.J, Prentice, C.S., Dawson, T.E., Seitz, G., Schwartz, D.P., Hudnut, K.W., Rosa, C., Pickering, A., and Parker, J.W., 2015, Tearing the terroir: Details and implications of surface rupture and deformation from the 24 August 2014 M6.0 South Napa earthquake, California: Earth and Space Science, v. 3, p. 416-430.

Dreger, D., M. Huang, A. Rodgers, T. Taira, and K. Wooddell (2015), Kinematic Finite-Source Model for the 24 August 2014 South Napa, California, Earthquake from Joint Inversion of Seismic, GPS, and InSAR Data, Seismological Research Letters, v. 86 no. 2, p. 327-334.

Donald Herzog and Associates, Inc., 1984, Report, soil investigation, Murdock Property, 1133 Larkin Way, Napa, California, DH&A Job No. 7026.1-0-3, California Division of Mines and Geology Alquist-Priolo File No. C-569.

Donnellan, A., Arrowsmith, R., Langenheim, V., 2015, Select airborne techniques for mapping and problem solving: in Anderson, R.L., and Ferriz, H., Applied Geology in California, Special Publication 26, Association of Environmental and Engineering Geologists, Chapter 30.

Engeo, 1977a, Geologic Investigation of Mill Valley Fault, Century Oaks Unit 4, Napa, California, Project No. N6-0905-B1, February 2, 1977.

Engeo, 1977b, Geologic Investigation of West Napa Fault, Mead Property, Napa County, California, Project No. N7-0834-B2, March 21, 1977, California Division of Mines and Geology Alquist-Priolo File No. C-352 (reassigned to No. C-265).

Engeo, 1978/1979b, Fault hazard investigation of Forest View subdivision, Napa, California, Project No. N8-1243-B1.

Engeo, 1979a, Seismic Hazards Exploration of the Herzog-Schroeder Property, near end of Pinewood Drive, Napa, California, Project No. N9-1381-B1, California Division of Mines and Geology Alquist-Priolo File No. C-397.

Field, E.H., Biasi, G.P., Bird, P., Dawson, T.E., Felzer, K.R., Jackson, D.D., Johnson, K.M., Jordan, T.H., Madden, C., Michael, A.J., Milner, K.R., Page, M.T., Parsons, T., Powers, P.M., Shaw, B.E., Thatcher, W.R., Weldon, R.J., II, and Zeng, Y., 2013, Uniform California earthquake rupture forecast, version 3 (UCERF3)—The time-independent model: U.S. Geological Survey Open-File Report 2013–1165, 97 p., California Geological Survey Special Report 228, and Southern California Earthquake Center Publication 1792, http://pubs.usgs.gov/of/2013/1165/.

Fox, K.F., Jr, Sims, J.D., Bartow, J.A., and Helley, E.J., 1973, Preliminary geologic map of eastern Sonoma County and western Napa County, California: U.S. Geological Survey Miscellaneous Field Studies Map MF-483, scale 1:62,500.

Fox, K.F., Jr., 1983, Tectonic setting of Late Miocene, Pliocene, and Pleistocene rocks in part of the Coast Ranges North of San Francisco, California: U.S. Geological Survey Professional Paper 1239, 33 p.

Graymer, R. W., E. E. Brabb, D. L. Jones, J. Barnes, R. S. Nicholson, and R. E. Stamski (2007), Geologic map and map database of eastern Sonoma and western Napa Counties, California, U.S. Geological Survey Scientific Investigations Map 2956, scale 1:100,000.

Helley, E.J. and Herd, D.G., 1977, Map showing Quaternary displacement, northeastern San Francisco Bay area region: U.S. Geological Survey Miscellaneous Field Studies Map MF-881, scale 1:125,000.

Herzog Associates, Inc., 1990, Geotechnical Investigation Report, Arden Manor Subdivision, Larkin-Scenic Property, Napa, California, Project No. 7696.02-01-3.

Hudnut, K.W., Brocher, T.M., Prentice, C.S., Boatwright, J., Brooks, B.A., Aagaard, B.T., Blair, J.L., Fletcher, J.B., Erdem, J.E., Wicks, C.W., Murray, J.R., Pollitz, F.F., Langbein, J., Svarc, J., Schwartz, D.P., Ponti, D.J., Hecker, S., DeLong, S., Rosa, C., Jones, B., Lamb, R., Rosinski, A., McCrink, T.P., Dawson, T.E., Seitz, G., Rubin, R.S., Glennie, C., Hauser, D., Ericksen, T., Mardock, D., Hoirup, D.F., and Bray, J.D., 2014, Key recovery factors for the August 24, 2014, South Napa earthquake: U.S. Geological Survey Open-File Report 2014–1249, 51 p., http://dx.doi.org/10.3133/ofr20141249

J.H. Kleinfelder & Associates, 1983, Fault Investigation Report, 3189 Laurel Street, Napa, California, File No. C-1402-1.

Jennings, C.W., and Bryant, W.B., 2010, Fault activity map of California: California Geological Survey, Geologic Data Map No. 6, scale 1:750,000.

Jim Glomb Consulting, 2015, Fault Investigation, Rafael Property, Napa, California, dated November 25, 2015, Project number 1472.

Jones, C. E., 2015, A practical guide to synthetic aperture radar interferometry for engineering and environmental geologists: in Anderson, R.L., and Ferriz, H., Applied Geology in California, Special Publication 26, Association of Environmental and Engineering Geologists, Chapter 31.

Joyce Associates, 1993, Fault Hazard Investigation of Stanly Ranch, Napa, California, Job Number 127.01, California Division of Mines and Geology Alquist-Priolo File No. C-961.

Langenheim, V.E., Graymer, R.W., and Jachens, R.C., 2006, Geophysical setting of the ML 5.2 Yountville, California Earthquake: Implications for seismic hazard in Napa Valley, California: Bulletin of the Seismological Society of America, v. 96, no. 3, p. 1192-1198.

Lienkaemper, J. J., DeLong, S. B., Domrose, C., and Rosa, C. M., 2016, Afterslip Behavior following the 2014 M 6.0 South Napa Earthquake with Implications for Afterslip Forecasting on Other Seismogenic Fault: Seismological Research Letters, v. 87, no. 3, p. 609-619.

Melgar, D., Geng, J., Crowell, B.W., Jaase, J.S., Bock, Y., Hammond, W.C., and Allen, R.M., 2015, Seismogeodesy of the 2014Mw6.1 Napa earthquake, California: Rapid response and modeling of fast rupture on a dipping strike-slip fault: Journal of Geophysical Research: Solid Earth, v. 120, p. 5013-5033.

Miller Pacific Engineering Group, 2014, Fault Trench Investigation, Irene M. Snow Elementary School, 1130 Foster Road, Napa, California, Project 936.181.

Moore & Taber, 1974a, Addendum to report of Preliminary Soils Investigation, Broadmoor Estates No. 3 dated March 5, 1974 (34/10P), Napa, California.

Moore & Taber, 1974b, Comments on Draft EIR, Hidden Valley Condominiums, Napa, California.

NASA, 2014, Advanced Rapid Imaging and Analysis (ARIA) Center for Natural Hazards Data: (accessed 10/2015 at: https://aria.jpl.nasa.gov/case_studies).

NASA, 2015, UAVSAR data: (accessed 10/2015 at http://uavsar.jpl.nasa.gov).

NCALM (2003), Napa Watershed, CA, doi:10.5069/G9BG2KW9.

Pampeyan, E.H., 1979, Preliminary map showing recency of faulting in coastal north-central California: U.S. Geological Survey, Miscellaneous Field Studies Map MF-1070, 13 pp. pamphlet, 3 sheets, scale 1:250,000.

Phoenix Geotechnical, 1994, Preliminary Geotechnical Feasibility Study, Napa Oaks Subdivision, Napa, California, Project No. 90-1-93.

Phoenix Geotechnical, 1996, Geotechnical Feasibility Report, Proposed property subdivision, 3201 Browns Valley Road, Napa, California, Project No. 221-1.

Phoenix Geotechnical, 1998, Addendum to Geotechnical Report, Response to EIR Comments, Proposed Tentative Map Submittal, Napa, California, Project No. 90-3.

Polcari, M., M. Palano, J. Fernandez, S. Samsonov, S. Stramondo, and S. Zerbini, 2016, 3D displacement field retrieved by integrating Sentinel-1 InSAR and GPS data: the 2014 South Napa earthquake: European Journal of Remote Sensing, v. 49, p. 1-13.

Ponti, D.J., Rosa, C., and Blair, J.L., 2017 (in press), Observations of ground deformation from the August 24, 2014 South Napa Earthquake: U.S. Geological Survey Open-File Report 2017-XXXX.

RGH Consultants, 2015a, Fault Study, Foothills Estates Subdivision, Foothill Boulevard, Napa, California, Project No. 3047.03.02.2.

RGH Consultants, 2015b, Geotechnical Study Report, Truchard Winery, 4062 Old Sonoma Road, Napa, California, Project No. 6838.01.04.2.

Rosen, P.A., S. Hensley, K. Wheeler, G. Sadowy, T. Miller, S. Shaffer, R. Muellerschoen, C Jones, H. Zebker. and S. Madsen, 2006, April. UAVSAR: A new NASA airborne SAR system for science and technology research. In 2006 IEEE Conference on Radar. 8p.

Rubin, R.S., Dawson, T.E., Mareschal, M., 2014, Pre-Earthquake Paleoseismic Trenching in 2014 Along a Mapped Trace of the West Napa Fault, Abstract S33F-4934 presented at 2014 Fall Meeting, AGU, San Francisco, Calif., 15-19 Dec.

Ryan Geological Consulting, Inc., 2015, Fault Investigation Report, Anthem Winery and Vineyards, LLC, 3454 Redwood Road, Napa, California, Job No. 1210.100.

Seitz, G., Ryan, K., and Rosa, C., 2015, Multiple Holocene-age events on the easternmost surface rupture of the August 24, 2014 South Napa Earthquake: Seismological Research Letters, v. 86, no. 2B, p. 634.

Taber Consultants, 1986, Preliminary Soils Investigation, Hillview Park Subdivision, Napa, California, Project No. 3P3/586/37-2.

TRC, 2008, Fault Investigation, 3075 Laurel Street, Napa, California, Report No. 2348-1/154871.

U.S. Geological Survey and California Geological Survey (2017), Quaternary fault and fold database for the United States, accessed July 7, 2017, from USGS web site: http//earthquake.usgs.gov/hazards/qfaults/

Wagner, D.L. and Bortugno, E.J., 1982, Geologic map of the Santa Rosa Quadrangle, California: California Division of Mines and Geology Regional Geologic Map Series Map 002A, scale 1:250,000.

Wagner, D.L., and Gutierrez, C.I., 2016, Preliminary geologic map of the Napa and Bodega Bay 30'x60' quadrangles, California: California Geological Survey, Preliminary Geologic Maps, scale 1:100,000.

Wesling, J.R., and Hanson, K.L., 2008, Digital compilation of West Napa fault data for the Northern California Quaternary Fault Map Database: Final Technical Report submitted to the U.S. Geological Survey NEHRP, Award no. 05HQAG0002, 61 pp.

Western Geological Consultants, 1979, Exploration Trench Data, 327 Foothill Blvd., Napa, CA, Assessor's Parcel 43-02-006, File No. 94-67-7, dated November 5, 1979.

Western Geological Consultants, 1980, Geologic Hazards Investigation, Mead Property, Browns Valley Road & Robinson Lane, Napa County, California, Project No. 94-47-7, dated January 8, 1980, California Division of Mines and Geology Alquist-Priolo File No. C-396.

Zwieback, S., Hensley, S., and Hajnsek, I., 2015, Assessment of soil moisture effects on L-band radar interferometry: Remote Sensing of Environment, v. 106, p. 77-89.

Table 1. Geomorphic analysis of mapped lineaments

Feature No.	Feature Type	Evaluation comment
1	scarp	Scarp is visible in the field and in lidar imagery, although not necessarily for the full length as mapped by Wesling and Hanson (2008). Feature #4 below reflects mapping from this FER.
2	Linear drainage, saddles, right step drainage, linear front	Features mapped by Wesling and Hanson (2008) are not evident in lidar. The drainage offset is indistinguishable from a meandering drainage pattern. 2014 rupture mapped to east, based on SAR imagery. See information regarding subsurface exploration in this area in Table 2, Site 3.
3	scarp	Based on the location in close proximity and subparallel to the Napa River, this feature is interpreted to be a fluvially cut terrace riser. Lidar topography improves the expression compared to aerial photos. Tonal lineaments mapped by Wesling and Hanson (2008) in this location appear to reflect land use boundaries on aerial photographs.
4	scarp	Scarp mapped to the extent visible in lidar. Approximate dimensions are 1.1 km long, 7 m high, and 50 to 100 m wide, based on lidar. Lidar profiles show scarp crest is rounded.
5	scarp	Scarp is up to 6 m high and 80 m wide in lidar profile. Similar to mapping by Wesling and Hanson (2008). Based on aerial photographs and lidar imagery, the scarp may be enhanced by fluvial erosion and/or cultural modification.
6	linear valley, vegetation contrast, scarp	Similar to mapping of Wesling and Hanson (2008), including west-facing scarp visible in lidar. Orientation of the feature may be consistent with bedrock structure. Association with tectonic features is unknown.
7	scarp	Scarp visible in lidar, mapped in-part as tonal contrast by Wesling and Hanson (2008). Scarp parallels geologic contact. Lidar profiles indicate scarp is up to 20 m high. Vegetation contrast varies in strength of expression over time.
8	linear valley	
9	tonal contrast	
10	linear front	NE-facing bedrock slope.
11	linear front	
12	linear valley	Broad feature, modified by development.

13	scarp	Scarp mapped by Wesling and Hanson (2008) is not evident in lidar.
14	linear valley	
15	linear valley	
16	scarp and tonal contrast	Scarp mapped by Wesling and Hanson (2008) is not evident in pre-development aerial photographs. Tonal is similar to observations in this FER.
17	linear valley	
18	linear front	
19	saddle	
20	linear valley	
21	saddle	
22	linear valley	
23	scarp	Scarp visible in pre-SNE lidar imagery along hillside.
24	linear valley	
25	linear valley	
26	saddle	
27	linear front	Feature is visible in pre-earthquake lidar imagery. Trench at northern end of feature exposed pre-2014 faults in Holocene deposits (Dawson et al., 2016); see Site # 4 in Table 2.
28	saddle	
29	saddle	
30	linear front	Feature is partially concealed by a landslide complex visible in lidar imagery.
31	saddle	Feature visible in lidar imagery and aerial photographs. A consulting trench across this feature encountered no faults. See Site #7 in Table 2 for additional information.
32	saddle	
33	saddle	
34	linear valley	
35	scarp, break in slope	Scarp mapped by Wesling and Hanson (2008) is not evident in lidar, but the break in slope to south is more apparent. Features may be obscured by artificial modifications visible in early aerial photographs and historic topographic map. See Site # 7 in Table 2 for additional discussion of subsurface investigation in this area.
36	saddle	
37	saddle, tonal contrast	

38	scarp	Scarp mapped by Wesling and Hanson (2008) is not evident in pre-development aerial photographs. Subtle irregularities in alluvial surface have an indeterminate origin.
39	right step drainage, linear front	Drainage offset is mapped by Wesling and Hanson (2008). However, observations in lidar imagery suggest a more continuous expression of possible scarps along the base of the fan to the east. Linear front is apparent in lidar imagery, although cultural modification appears to enhance the expression.
40	side hill bench	
41	side hill bench, tonal contrast	
42	linear ridge	
43	tonal contrast	
44	linear valley	
45	saddle	
46	Linear front	Spur ridges are observed to be faceted or truncated in lidar imagery, with additional notches on the ridgelines up slope to the east. Wesling and Hanson (2008) map similar features. Geomorphic expression is partially obscured by extensive cultural development.
47	saddle	
48	linear valley	
49	scarp	Scarps mapped with lidar along bedrock slopes above valley. Line is mapped to be partially coincident with fault encountered at Site 12, Table 2.
50	scarp	Scarp mapped using lidar, similar to mapping of Wesling and Hanson (2008).
51	saddle	
52	scarp?	Queried scarp mapped by Wesling and Hanson (2008) adjacent to creek. Feature could be consistent with a creek meander and fluvial terrace riser. Scarp to south is not evident in lidar.
53	linear front	Linear front appears to be associated with contact between bedrock and alluvium. Scarp mapped by Wesling and Hanson (2008) not shown on Plate, but similar to mapping from this FER.
54	right step drainage	Drainage offset mapped by Wesling and Hanson (2008) is not evident in pre-development aerial photographs. A discrete offset is not discernable from the meandering drainage pattern.

55	saddle	
56	saddle	See Site #19 in Table 2 for additional information about subsurface investigation of this feature.
57	several scarps	West-facing scarps sub-parallel to range front are mapped by Wesling and Hanson (2008), although lidar imagery suggests slight difference in locations. Form and location are consistent with either fluvial or tectonic origin. See Site #'s 19 and 21 in Table 2 for additional information on subsurface investigation in this area.
58	saddle	
59	linear front	Linear front appears to be associated with contact between bedrock and alluvium.
60	linear front	Similar to mapping of Wesling and Hanson (2008), however, limited to shorter more linear expression based on lidar imagery.
61	saddle	
62	topographic escarpment, bedrock fault	Topographic escarpment, closed depression, and bedrock fault mapped by Wesling and Hanson (2008). 2014 rupture trends across the lineament, rather than being coincident or parallel with it.
63	linear front	Linear front mapped by Wesling and Hanson (2008) appears to be associated with contact between bedrock and alluvium.
64	linear front	East-facing linear front sub-parallel to range front based on lidar. Similar to scarp mapped by Wesling and Hanson (2008). See Site #22 for additional information on subsurface investigation in this area.
65	scarp	
66	scarp	Scarp mapped along base of slope using lidar. Similar to mapping by Wesling and Hanson (2008). The curvilinear form may indicate enhancement by fluvial erosion. A trench exposure at the base of slope exposed depositional contacts, but no faults (Rubin et al., 2014). See two entries for Site 25, Table 2 for additional discussion of subsurface information at this location.
67	scarp	
68	scarp	
69	linear front, modified	
70	tonal contrast	
71	saddle	

72	right step drainage, scarp	Drainage offset and scarp mapped by Wesling and Hanson (2008). Offset is visible in early aerial photographs. In lidar views, recent incision and artificial modification are evident at the offset. Scarp is nearly coincident with alignment of Dry Creek Road, which has cut/fill modifications. Lidar profiles indicate a vertical step between higher and lower surfaces across the road alignment.
73	right step drainage	Drainage offset mapped by Wesling and Hanson (2008) is not discernable from a meandering pattern in lidar. Lineament is not on-trend with other features. See site # 26 in Table 2 for more information about subsurface investigation at this location.
74	tonal contrast	
75	tonal contrast	
76	saddle	
77	linear front	Similar location to of drainage offset mapped by Wesling and Hanson (2008). No offset is observed in lidar or early aerial photographs.
78	right step drainage	Drainage offset mapped by Wesling and Hanson (2008) is not evident in aerial photographs or lidar. Early aerial photographs show extensive artificial modification.
79	right step drainage	Drainage offset mapped by Wesling and Hanson (2008) is not evident in lidar or early aerial photographs. Extensive artificial modification limits interpretation.
80	tonal contrast	
81	linear front	
82	saddle	
83	tonal contrast	
84	tonal contrast	
85	tonal contrast	
86	right step drainage	Drainage offset mapped by Wesling and Hanson (2008) is coincident with extensive artificial modification, which is visible in early aerial photographs. Interpretation of pre-development configuration is significantly limited. Lineament is not on trend with others features.
87	linear front	Linear front similar to scarp mapped by Wesling and Hanson (2008), but limited to shorter more linear expression based on lidar. Bedrock exposed in road cut on west side indicates topography may be controlled by bedrock/alluvium contact. Orientation and extent of feature could be consistent with fluvial erosion.

88	right step drainage	Drainage offset mapped by Wesling and Hanson (2008) is part of channel with extensive artificial modification. Lineament is not on trend with others features.
89	tonal contrast	
90	right deflected ridge	Deflected ridge mapped by Wesling and Hanson (2008) is visible in lidar. However, landslides visible on either side of ridge contribute to the curved appearance, and other offset features are not observed on trend.
91	linear valley	
92	linear valley	
93	scarp?	Scarp mapped by Wesling and Hanson (2008) is not evident in lidar profiles.
94	tonal contrast	Tonal contrast mapped by Wesling and Hanson (2008) is not evident aerial photographs.
95	right step drainage	Drainage offset mapped by Wesling and Hanson (2008) is not evident in lidar or aerial photographs. A discrete offset is not discernable from the meandering drainage pattern.
96	tonal contrast	Tonal contrast mapped by Wesling and Hanson (2008) not evident aerial photographs.
97	linear ridge	
98	right step drainage	Drainage offset mapped by Wesling and Hanson (2008) is not evident in lidar.
99	scarp	Scarp mapped by Wesling and Hanson (2008) is not evident in lidar profiles.

Table 2. Summary of available fault investigation reports

Site No.	Reference (AP File #, if assigned)	Reported Conclusions	Evaluation comments
1	Wesling and Hanson, 2008 (1)	Holocene faulting identified at Napa Co. Airport trench site. Trench site selected based on geomorphic expression of fault.	
2	Dawson et al. 2016 (1)	Trench across Rupture Trace A; multiple previous rupture events, but insufficient Holocene deposition for pre-SNE event characterization.	
3	RGH Consultants, 2014a	Preliminary field study including two trenches excavated across faults mapped by Wesling and Hanson (2008). Steeply dipping bedrock exposed in trenches, but no evidence of faulting.	Report and log not available (Jared Pratt, pers comm.).
3	RGH Consultants, 2016	Trenches shadow proposed building footprint from projections of previously mapped faults or lineaments. No evidence of faulting encountered.	Logs not available.
3	Joyce Associates, 1993 C-961	Two trenches across previously mapped faults and lineaments. Minor shearing within Eocene bedrock identified, no evidence of faulting in overlying alluvium. Setbacks recommended for lineaments that were not explored, although those are located generally off-site.	
4	Dawson et al., 2016 (2)	Two trenches across Rupture Trace A and scarp. Several faults encountered, with evidence consistent with pre-SNE deformation. Stratigraphy not favorable to recognizing event history, but faulted deposits are Holocene in age.	

5	RGH Consultants, 2015b	Two trenches located across Rupture Trace C expose fault deformation in bedrock and overlying deposits. Setbacks are recommended from identified faults.	
6	Miller Pacific, 2014	Several trenches located across and near a fault previously mapped by Clahan et al. (2004). Faults and deformation are recognized in bedrock, with some zones extending short distances on-trend. Faulting of overlying soils was not recognized. However, based on the lack of data to preclude Holocene movement, setbacks are recommended from recognized faults.	
7	Seitz et al., 2015	Paleoseismic trench study: 3 events pre-dating SNE (2 in the Holocene), where significantly greater vertical displacements were observed.	
7	Berlogar, Stevens Associates, 2014	Several trenches in the western portion of the site are located to cross previously mapped faults and the SNE rupture. Consultants conclude western-most previously mapped fault has latest Pleistocene movement based on estimated soil ages in Trench 6. The consultants note deformation from the deeper fault zone extends higher in the section, although offsets are not observed. Setbacks are recommended along both the western fault zone and SNE rupture zone.	A radiocarbon date of approximately 25 ka from the lower faulted deposit was subsequently obtained by Seitz (pers. comm. 2017). The upper soils are not dated, and although offsets are not observed, this could be the result of lateral deformation and the shallow depths could be consistent with Holocene movement.

7	Phoenix Geotechnical, 1994	Several trenches located across previously mapped faults. Faults mapped on the eastern side of site were not identified in the trenches. Bedrock exhibits local shears, however the consultants conclude they are not continuous on strike and evidence of active faulting is absent. On western side of site, setbacks are recommended based on a continuous zone faulting recognized in trenches along a fault mapped by Helley and Herd (1977).	Subsequent investigation by Berlogar Stevens Associates (described above) provides additional data on location and activity of fault zone along western portion of site.
7	Phoenix Geotechnical, 1998	Three trenches excavated across mapped faults and lineaments at foot of rangefront in the northeastern portion of site. Deformation in bedrock is described as minor and localized, and is overlain by undeformed soils of estimated pre-Holocene age. Bedrock deformation at western end of trenches not continuous on-strike between trenches, although setbacks are recommended based on the inability to preclude displacement of Holocene soils in that portion of trench.	Logs not included in report, but detailed descriptions and soil analysis are reported.
8	RGH Consultants, 2015a	Trench excavated across fault mapped by Clahan et al. (2004), and near a fault mapped by Fox et al. (1973). No evidence of faulting was encountered in the trench.	
9	Western Geological Consultants, 1979	Two trenches excavated across the break in slope at range front, and a geophysical anomaly. No faults were encountered in the trenches, and the anomaly was found to be related to a section of bedrock covered with alluvium.	

10	TRC, 2008	Two trenches across fault mapped by Clahan et al. (2004). A fault zone was exposed within bedrock in both trenches. Faulting was not observed in overlying soil, however the consultants were unable to establish the soil age. Based on the inability to preclude Holocene movement, setbacks from the fault were recommended.	
11	J. H. Kleinfelder Associates, 1984	Six trenches across/near several mapped faults on range front. Bedrock is exposed in trenches, with no faulting observed.	
12	Western Geological Consultants, 1980 C-396	Trench located to cross previously mapped faults. A fault displacing the bedrock/soil interface is encountered, and consultants recommend setbacks based on displacement of soil interpreted to be young.	Trench crosses geomorphic scarp. Fault is identified up from the base of slope.
13	Taber Consultants, 1986	One trench excavated across fault mapped by Helley and Herd (1977), and nearly on-trend with fault encountered in Site 12 to south. Setback recommended from southwest property corner.	Report and log not available, but the lack of faults on the site plan within the trenched area suggests no faults were encountered.
14	Wesling and Hanson, 2008 (2)	Faulted Holocene alluvium reported at natural exposure in Browns Valley Creek at rangefront. Charcoal ages were obtained.	Could not verify faulting relationships at creek exposure during two field visits that included three other geologists (W. Bryant, T. Dawson, and J. Wesling).
15	Phoenix Geotechnical, 1996	Two trenches across fault mapped by Fox et al. (1973). No evidence of faulting reported within alluvial deposits, although deep fill is present in the eastern portion of site.	Deep fill may have precluded observation of geologic conditions, but this is not clear in the report. Trench logs are not included in the report.

16	Donald Herzog Associates, 1984 C-569	Two test pits encountered fault zone in bedrock. Though colluvial soils were not shown to be faulted, consultants recommend setbacks from the faults based on an assumed youthful soil age.	
17	Herzog Associates, 1990	Trenches excavated across faults projected from Site 16 to the southeast, as well as other previously mapped faults.	Though no evidence of faulting is interpreted by the consultants, features permissive of faulting are present on the Trench 4 log. Additionally, a bedrock contact identified as faulted at Sites 18 and 19 to the northwest likely exists between Trenches 5/6 and 7, based on unit descriptions from those trenches.
18	Engeo, 1977b C-265	Trench exposes fault mapped by Fox et al. (1973). Consultants interpret young soils displaced by fault, and recommend setbacks from the fault.	
19	Engeo, 1979a C-397	Three trenches near faults mapped by Fox et al. (1973) and Helley and Herd (1977). Deformed bedrock exposed in two trenches, soil involved in one of those. Fault separates bedrock units. Consultants interpret young soils displaced by fault, and recommend setbacks from the fault.	Consultant later re-interpreted faulted soil as non-tectonic (cited in Bryant, 1982).
20	RGH Consultants, 2014b	Test pit across open crack on Rupture Trace A; crack does not extend downward through base of soil. Bedrock not deformed.	Observed excavated pit. Consulting report not completed.
21	Engeo, 1977a	Trench excavated across fault mapped by Fox et al. (1973). No faults found, however, consultants interpret the existence of the fault offsite to the east and recommend setbacks from the property line.	

22	Moore and Taber, 1974b	One trench across or near mapped faults. No faulting observed in trench.	Conclusions verified in field during City Geologist and USGS peer reviews.
23	Moore and Taber, 1974a	Trenches address City Geologist concerns of nearby faulting mapped by Fox et al. (1973). Trench 1 crosses zone of SNE deformation. Trench 3 exposes bedrock contact. Consultants conclude contact is depositional.	SNE deformation ~110-130 west of contact in Trench 3. Unit descriptions from report appear consistent with depositional contact between GVG and Domengine Formation bedrock units in Trench 3.
24	Prentice et al., 2015	Several trenches across Rupture Traces A and C at Hendry Vineyard. Trenches within ~6k yr. old deposits yield no evidence of faults. Trenches on likely Pleistocene-age terrace reveal faults of unconstrained age, with vertical offsets of ~ 2 m or less.	
25	Clahan et al., 2011	Holocene faulting interpreted in natural stream exposure, at base of scarp in eastern Alston Park.	Subsequent trenching at this location by Rubin et al. (2014) indicates only depositional contacts at this location (see below).
25	Rubin et al., 2014	Trench at Eastern Alston Park crosses base of scarp and previously mapped faults. Trench shadowed creek exposure interpreted by Clahan et al. (2011). Quaternary or older materials exposed in trench, with no faults encountered; only depositional contacts.	
26	Jim Glomb Consulting, 2015	Trench shadows alignment of fault mapped by Wesling and Hanson (2008). Trench exposed bedrock, with no evidence of faulting encountered.	
27	Engeo, 1978/1979b	Two trenches located to cross fault mapped by Fox et al. (1973). No evidence of faulting encountered in trenches.	

28	Ryan Geological Consulting, 2015	Several trenches located to cross SNE fissures, UAVSAR lineament of Ponti et al. (2017), and fault mapped by Fox et al. (1973). Consultant concludes no faulting present in trenches. Fissures found above steeply dipping bedrock in subsurface, but do not extend downward beyond the soil. Consultant concludes surface cracks are ridge-top spread features, or related to settlement of utility trench backfill.